1974

Analytical Analysis of the Forced Vibration of the Sprung Mass of a Reciprocating Hermetic Compressor, Including comparison with Experiment

G. W. Gatecliff
Tecumseh Products Company

ANALYTIC ANALYSIS OF THE FORCED VIBRATION OF THE SPRUNG MASS OF A RECIPROCATING HERMETIC COMPRESSOR, INCLUDING COMPARISON WITH EXPERIMENT

George W. Gatecliff, Ph.D., Chief Research Engineer
Tecumseh Products Research Laboratory, Ann Arbor, Michigan

ABSTRACT

A mathematical analysis is made of compressor motion within a housing as a function of design and operating parameters. The forces considered include pressure forces, inertia forces, unbalance forces due to crankshaft eccentricity and counterweights, and restoring forces exerted by the mounting springs. The governing equations are obtained by applying the linear and rotational form of Newton's Second Law in each of three mutually perpendicular directions. The solution of the steady-state portion of the problem yields the linear and angular displacement and velocity of the sprung mass about each axis as a function of crankshaft position.

The instrumentation used to measure the vibration of the sprung mass relative to the housing is described and experimental traces illustrating the vibratory motion are presented.

INTRODUCTION

High-speed hermetic compressors are designed and manufactured for many years of dependable, maintenance-free service. Particular attention must be paid to the design of the mounting system to insure conditions of load compatible with long life and noiseless operation. The dynamic characteristics of the piston/connecting rod/crankshaft linkage, the pressure forces within the cylinder, and the flexural characteristics of the suspension system bear directly on this problem. A model incorporating each of these aspects offers a means of seeking a balance between the conflicting requirements for a suspension with sufficient flexibility to produce quiet operation and adequate stiffness to prevent objectionable transient behavior when operation ceases.

MATHEMATICAL MODEL

The slider-crank mechanism consists of a piston, connecting rod and crankshaft as shown in Fig. 1 for the purpose of analysis. Its motion is determined by the force exerted on the piston, P, the torque applied to the rotor, T, and the physical constants describing the system. The ideal

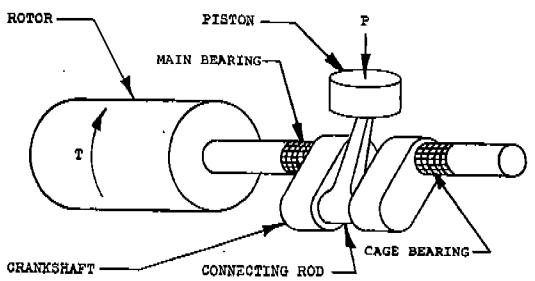

Fig. 1 Slider-crank mechanism

pressure-volume diagram provides a means of calculating cylinder pressure as a function of crankshaft position consistent with the accuracy required here.

Beginning with the free body diagram of the piston shown in Fig. 2, the following equations result:

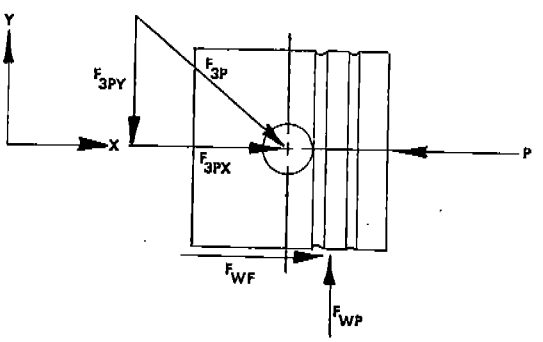

Fig. 2 Free body diagram of piston

$$F_X = MA_X;\ F_{3PX} + F_{WP} - P = M_P A_P \quad (1)$$

$$F_Y = MA_Y;\ F_{WP} - F_{3PY} = 0 \quad (2)$$

The analysis outlined below applies for the free body diagram of the connecting rod shown in Fig. 3.

$$\sum F_X = MA_X;\ F_{23X} - F_{3PX} = M_{CR} A_{CGX} \quad (3)$$

$$\sum F_Y = MA_Y;\ F_{23Y} + F_{3PY} = M_{CR} A_{CGY} \quad (4)$$

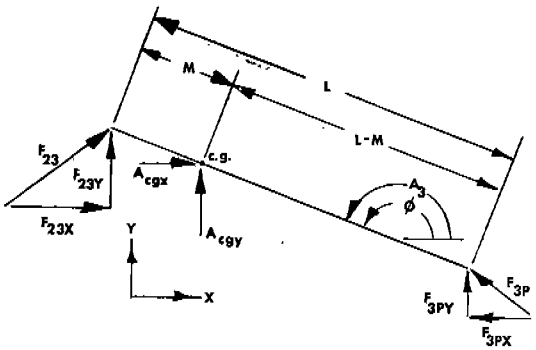

Fig. 3 Free body diagram of connecting rod

$$\sum T_{CG} = IA;\ F_{3PY}(L-M)\cos(180-\phi) - F_{3PX}(L-M)\sin(180-\phi) - F_{23Y}M\cos(180-\phi) - F_{23X}M\sin(180-\phi) = I_{CR}A_3 \qquad (5)$$

For the free body diagram of the crankshaft rotor assembly shown in Fig. 4:

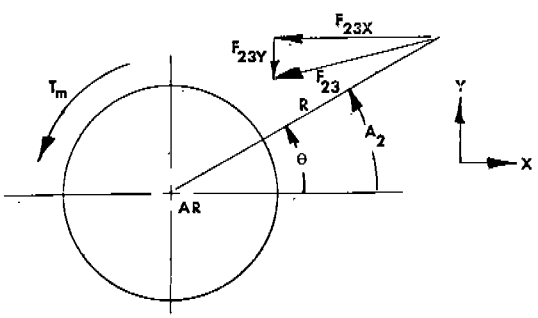

Fig. 4 Free body diagram of crankshaft rotor assembly

$$\sum T_{AR} = IA;\ F_{23X}R\sin\theta - F_{23Y}R\cos\theta + T = I_{CSR}A_2 \qquad (6)$$

Utilizing the following kinematic relationships by Cowie (1), it is apparent that ø, w_3 and A_3, and therefore A_{CGX}, A_{CGY} and A_P are expressible as functions of θ, w_2, A_2, R, L, and M for the linkage pictured in Fig. 5.

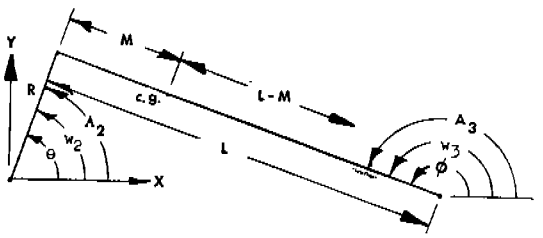

Fig. 5 Kinematic conventions for slider-crank mechanism

$$\phi = \text{Arcsin}\ (R/L)\sin\theta$$

$$w_3 = R\cos\theta\, w_2/L\cos\phi$$

$$A_3 = (w_3^2 - w_2^2)\tan\phi + (w_3/w_2)A$$

$$X_{CG} = R\cos\theta - M\cos\phi$$

$$Y_{CG} = R\sin\theta - M\sin\phi$$

$$V_{CGX} = M\, w_3\sin\phi - R\, w_2\sin\theta$$

$$V_{CGY} = (\,(L-M)/L)\, R\, w_2\cos\theta$$

$$A_{CGX} = M(A_3\sin\phi + w_3^2\cos\phi) - R(A_2\sin\theta + w_2^2\cos\theta)$$

$$A_{CGY} = (\,(L-M)/L)R(A_2\cos\theta - w_2^2\sin\theta)$$

$$X_P = R\cos\theta - L\cos\phi$$

$$V_P = L\, w_3\sin\phi - R\, w_2\sin\theta$$

$$A_P = L(A_3\sin\phi + w_3^2\cos\phi) - R(A_2\sin\theta + w_2^2\cos\theta)$$

Upon examination of these relations, it is apparent that for known values of P, T, θ and w_2, the analysis of the slider-crank reduces to the solution of five simultaneous linear equations in terms of the variables F_{3PX}, F_{3PY}, F_{23X}, F_{23Y} and A_2.

Applicability of this procedure arises from the continuous nature of the slider-crank motion and can be made as accurate as desired by choosing smaller and smaller values of Δθ. In practice, a value of Δθ equal to 2 crankshaft degrees of rotation permits the assumption of constant angular acceleration between steps, thereby allowing the amount of time t required to advance Δθ degrees to be calculated as follows:

$$t = \frac{-w_{2I} + \sqrt{w_{2I}^2 + 2\Delta\theta A_{2I}}}{A_{2I}} \quad \text{for } A_{2I} \neq 0$$

or

$$t = \Delta\theta/w_{2I} \quad \text{for } A_{2I} = 0$$

The angular velocity at the end of time increment t is determined by the following relationship:

$$w_2 = A_{2I}t + w_{2I}$$

Once w_2 and A_2 are known as functions of θ, the X and Y components of the forces associated with unbalance sections of the crankshaft may be calculated. The following equations apply for the unbalanced mass depicted in Figure 6:

$$F_R = m_U e_U w_2^2$$

$$F_T = m_U e_U A_2$$

$$F_{XU} = F_R \cos(\theta+\psi) + F_T \sin(\theta+\psi)$$

$$F_{YU} = F_R \sin(\theta+\psi) - F_T \cos(\theta+\psi)$$

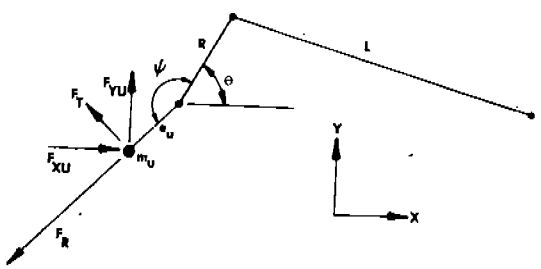

Fig. 6 Schematic diagram of an unbalanced mass

The resultant X-direction force in the bearings at each position in the cycle is given by the expressions which follow. They are obtained by summing moments about the main and cage (outboard) bearings respectively.

$$FCBX = -\sum_{I=1}^{N} \frac{F_{XI}^{I} D_I - F_{23X} DT}{DBB}$$

$$FMBX = -\sum_{I=1}^{N} \frac{F_{XU}^{I}(DBB-D_I) - F_{23X}(DBB-DT)}{DBB}$$

Similarly, for the Y-direction:

$$FCBY = -\sum_{I-1}^{N} \frac{F_{YU}^{I} D_I - F_{23Y} DT}{DBB}$$

$$FMBY = -\sum_{I=1}^{N} \frac{F_{YU}^{I}(DBB-D_I) - F_{23Y}(DBB-DT)}{DBB}$$

The time-varying pressure, cylinder wall, and bearing forces obtained from this analysis are the disturbances giving rise to the vibratory motion of the sprung mass of the compressor. Fig. 7 shows the geometric relationship between the point of application of the various forcing functions and the center of gravity of the sprung mass. The distance XC varies according to the following relationship:

$$XC = X_p - XB$$

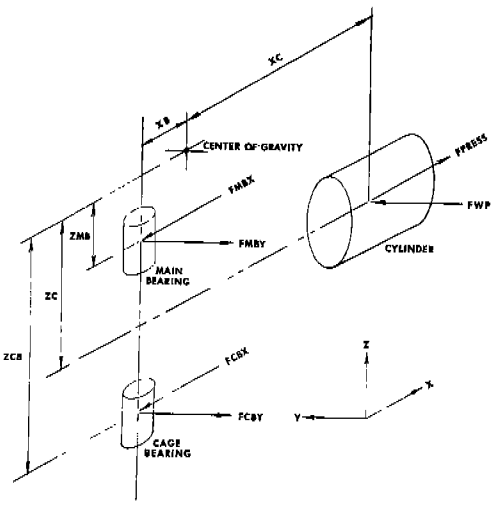

Fig. 7 Free body diagram of mechanism and pressure forces acting on the sprung mass of the compressor

The geometric relationship of the forces exerted on the sprung mass of the compressor by the suspension system is depicted in Fig. 8.

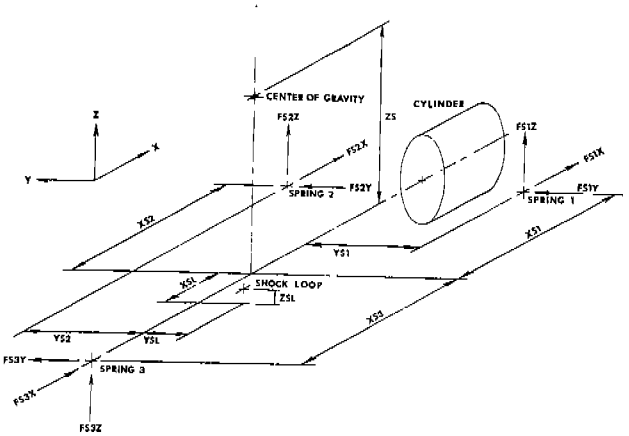

Fig. 8 Free body diagram of suspension system forces acting on the sprung mass of the compressor

The following relationships result from the application of the linear and rotational form of Newton's Second Law in the X, Y and Z directions about the center of gravity of the sprung mass:

$$\sum F_X = 0;\ -FMBX - FCBX + FPRESS + FS1X + FS2X + FS3X + FSLX - m\ddot{X} = 0 \qquad (7)$$

$$\sum F_Y = 0; \quad -FMBY - FCBY + FW + FS1Y + FS2Y + FS3Y + FSLY - m\ddot{Y} = 0 \tag{8}$$

$$\sum F_Z = 0; \quad FS1Z + FS2Z + FS3Z + FSLZ - m\ddot{Z} = 0 \tag{9}$$

$$\sum M_X = 0; \quad -FMBY\ ZMB + FW\ ZC - FCBY\ ZCB - FS1Z\ YS1 + FS2Z\ YS2 + FS1Y\ ZS + FS2Y\ ZS + FS3Y\ ZS - FSLZ\ YSL + FSLY(ZS - ZSL) - I_X\ddot{e}_X = 0 \tag{10}$$

$$\sum M_Y = 0; \quad FMBX\ ZMB + FCBX\ ZCB - FPRESS\ ZC - FS1Z\ XS1 - FS2Z\ XS2 + FS3Z\ XS3 - FS1X\ ZS - FS2X\ ZS - FS3X\ ZS + FSLZ\ XSL - FSLX(ZS - ZSL) - I_Y\ddot{e}_Y = 0 \tag{11}$$

$$\sum M_Z = 0; \quad FMBY\ XB + FCBY\ XB + FW\ XC + FS1Y\ XS1 + FS2Y\ XS2 - FS3Y\ XS3 + FS1X\ YS1 - FS2X\ YS2 - FSLY\ XSL + FSLX\ YSL - T - I_Z\ddot{e}_Z = 0 \tag{12}$$

Utilizing the following relationships which are approximately true for small displacements about the mean and collecting terms, the problem reduces to the solution of six nonhomogeneous coupled second-order linear differential equations:

$$FPRESS = \pi R_C^2 (P_{CYL} - P_{SUC}) \tag{13}$$

$$FS1X = -KS1X\ (X + YS1\ e_Z - ZS\ e_Y) \tag{14}$$

$$FS1Y = -KS1Y\ (Y + XS1\ e_Z + ZS\ e_X) \tag{15}$$

$$FS1Z = -KS1Z\ (Z - YS1\ e_X - XS1\ e_Y) \tag{16}$$

$$FS2X = -KS2X\ (X - YS2\ e_Z - ZS\ e_Y) \tag{17}$$

$$FS2Y = -KS2Y\ (Y + XS2\ e_Z + ZS\ e_X) \tag{18}$$

$$FS2Z = -KS2Z\ (Z + YS2\ e_X - XS2\ e_Y) \tag{19}$$

$$FS3X = -KS3X\ (X - ZS\ e_Y) \tag{20}$$

$$FS3Y = -KS3Y\ (Y - XS3\ e_Z + ZS\ e_X) \tag{21}$$

$$FS3Z = -KS3Z\ (Z + XS3\ e_Y) \tag{22}$$

$$FSLX = -KSLX\ (X + YSL\ e_Z - (ZS - ZSL)\ e_Y) \tag{23}$$

$$FSLY = -KSLY\ (Y - XSL\ e_Z + (ZS - ZSL)\ e_X) \tag{24}$$

$$FSLZ = -KSLZ\ (Z - YSL\ e_X + XSL\ e_Y) \tag{25}$$

The resulting formulation may be written as follows using matrix notation:

$$[M]\{\ddot{n}\} + [K]\{n\} = \{F\} \tag{26}$$

where

$n(1) = X$

$n(2) = Y$

$n(3) = Z$

$n(4) = e_X$

$n(5) = e_Y$

$n(6) = e_Z$

and

$M_{ij} = 0$ for $i \neq j$

$M_{11} = M_{22} = M_{33} = m$

$M_{44} = I_X$

$M_{55} = I_Y$

$M_{66} = I_Z$

$F(1) = -FMBX - FCBX + FPRESS$

$F(2) = -FMBY - FCBY + FW$

$F(3) = 0$

$F(4) = -FMBY\ ZMB - FCBY\ ZCB + FW\ ZC$

$F(5) = +FMBX\ ZMB + FCBX\ ZCB - FPRESS\ ZC$

$F(6) = +FMBY\ XB + FCBY\ XB + FW\ XC - T$

and the individual values of K_{ij} are found by substituting equations 13 - 25 in equations 7 - 12 and collecting terms.

The steady periodic behavior of the sprung mass under given operating conditions may be obtained with the aid of a Fourier series representation of the forcing functions in the column matrix $\{ F \}$ over the period of one crankshaft revolution. The problem reduces to the following form utilizing this technique:

$$[M] \{\ddot{n}\} + [K] \{n\} = \left\{ \sum_{j=1}^{b} A_j \sin w_j t + \sum_{j=1}^{b} B_j \cos w_j t \right\}$$

A complete presentation of the details associated with the solution of this formulation may be found in Meirovitch (2). Figs. 9 - 14 show the calculated results for a typical case.

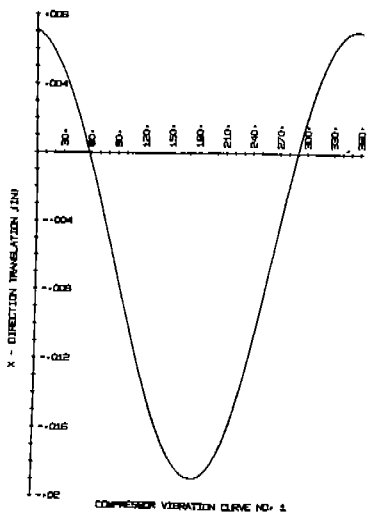

Fig. 9

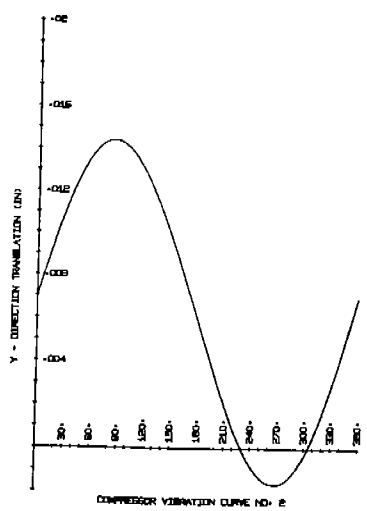

Fig. 10

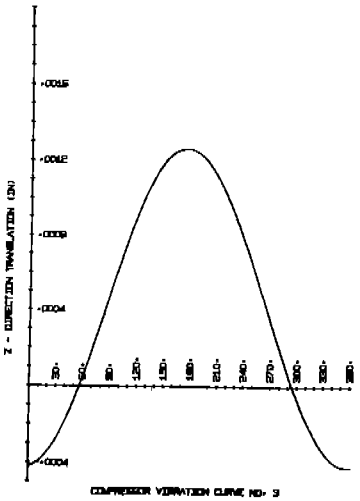

Fig. 11

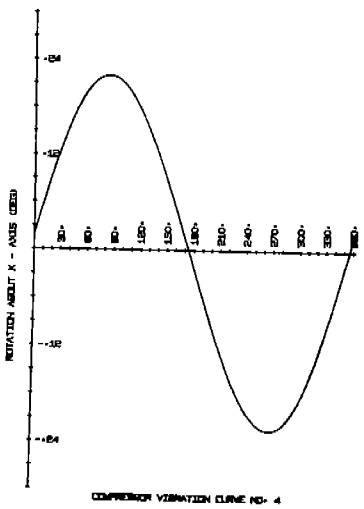

Fig. 12

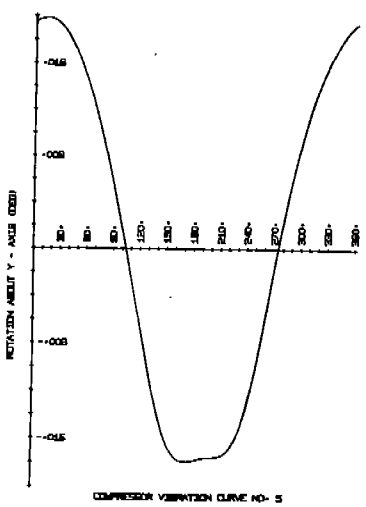

Fig. 13

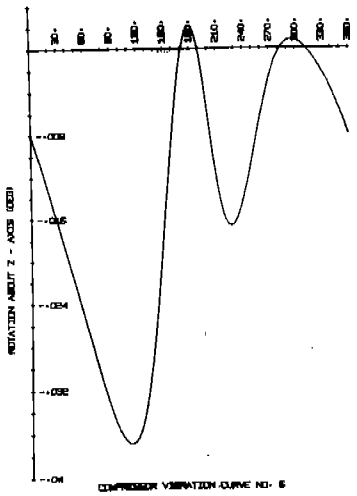

Fig. 14

EXPERIMENTAL DATA

Experimental measurements were conducted utilizing a light cell to measure the vibratory motion of the sprung mass. A small projection was attached to the crankcase and the relative motion between the sprung mass and the shell was sensed by measuring the travel of the projection's shadow back and forth across the light cell. Fig. 15 shows a highly simplified schematic diagram of this apparatus.

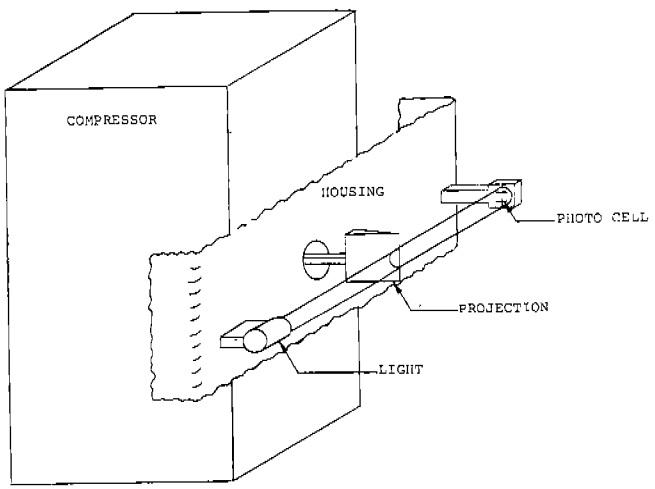

Fig. 15

A sample of the output from this transducer illustrating the X-direction translation is shown in Fig. 16. The scale is such that each major division on the picture represents 0.0068 in. of movement between the sprung mass and the shell. As a result, Fig. 16 indicates a peak-to-peak travel of 0.0204 in., compared to a calculated value of 0.0260 depicted in Figure 9.

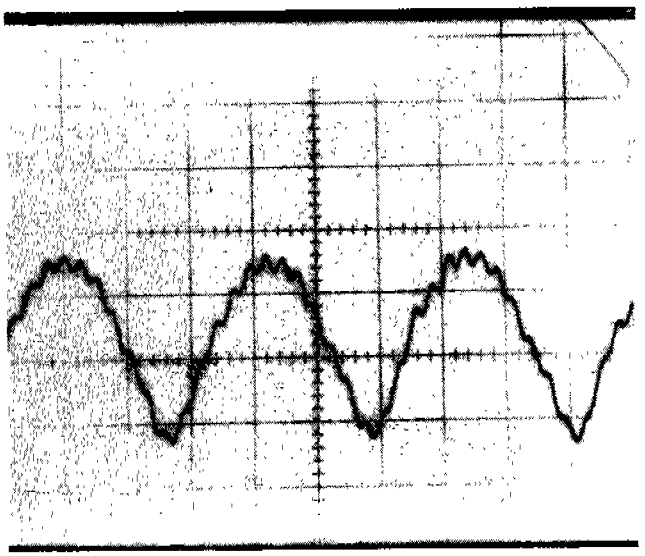

Fig. 16

The most obvious difference between Figs. 9 and 16 is the substantial amount of high frequency content in the experimental trace. In an effort to ascertain the predominant frequencies of the trace in Fig. 16, the wave form was passed through a filter capable of eliminating all frequencies with the exception of those between preset limits. Figs. 17 and 18 were produced in this way.

Fig. 17 displays the original wave form together with the contribution to the wave. form from vibrations between 40 and 95 Hz. The compressor was operating at a crankshaft frequency of 56.7 Hz. during the time Figs. 17 and 18 were recorded. As a

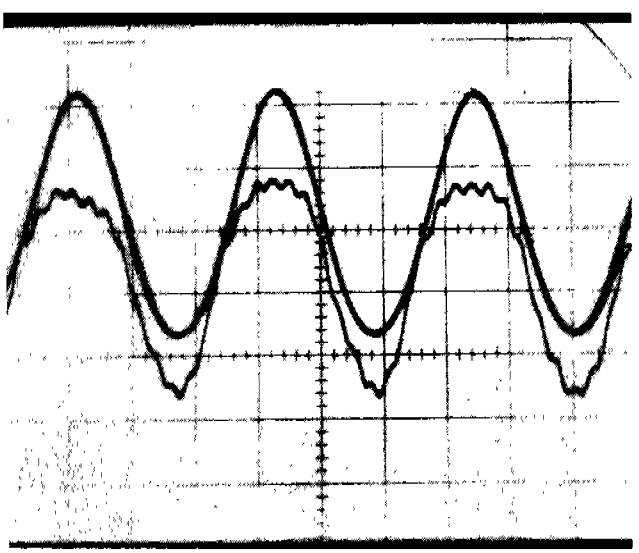

Fig. 17

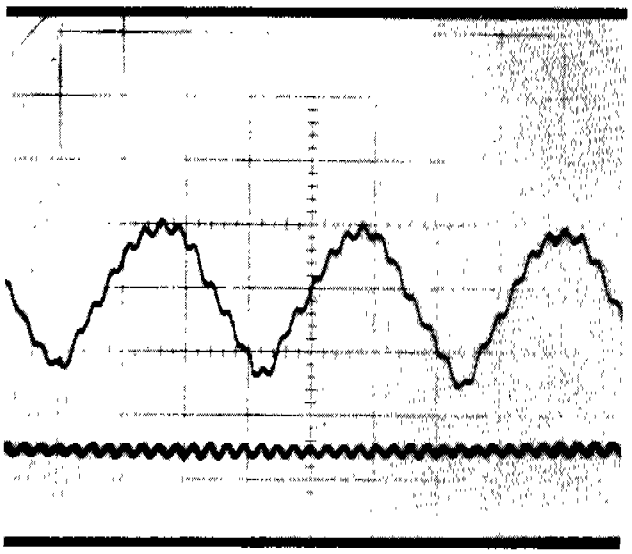

Fig. 18

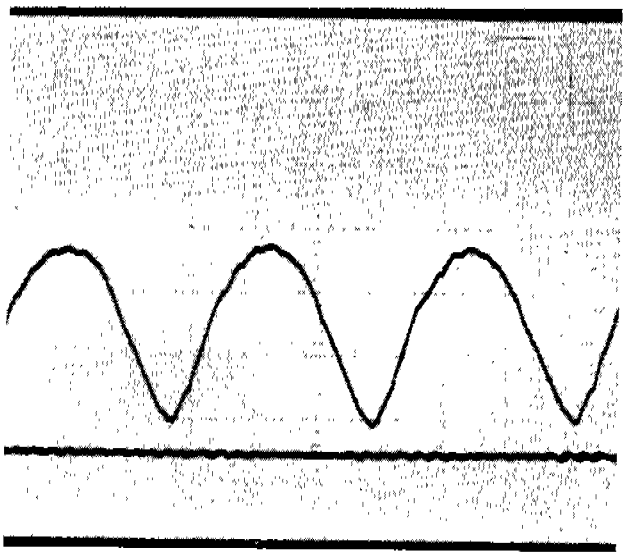

Fig. 19

result, Fig. 17 depicts the original wave form on the bottom and the fundamental component on the top. The peak-to-peak height of this trace is 0.0272 in. which compares favorably with the 0.0260 in. distance shown in Fig. 9.

Fig. 18 depicts the original wave form together with the contributions to the wave form from vibrations with frequencies between 600 and 1000 Hz. Frequencies within this range are often associated with a higher-order vibratory mode of the shell. It may be noted that there are 12 cycles of the higher frequency vibration within each cycle of the fundamental. As a result, a shell vibrating at this frequency would have 12 nodes and 12 antinodes about its periphery.

A clamp placed across the shell such that the two contact points do not fall on antinodes and are separated by six cycles of vibration should substantially modify this motion. Fig. 19 depicts the transducer output with the shell clamped in this manner.

The audible noise associated with the test unit dropped noticeably with the clamp in place. This, together with the measurable difference between Fig. 18 and 19, was taken as verification that the high frequency component of the transducer trace was a result of shell vibration. Using the upper trace of Fig. 18, it appears the peak-to-peak amplitude of the shell at the location of the ransducer was 0.00136 in.

CONCLUDING REMARKS

The work described herein is little more than a start on an involved problem. The initial results are neither so precise that improvement is impossible nor so inexact as to be valueless. The calculation sequence is a small part of a larger study to evaluate the suspension forces contributing to shell vibration just as the slider-crank model (3) is a subpart of this effort. Much remains for future consideration including the subject of transient response.

LIST OF SYMBOLS

A_{CGX} Acceleration of the connecting rod center of gravity in the X-direction

A_{CGY} Acceleration of the connecting rod center of gravity in the Y-direction

A_P Acceleration of the piston in the X-direction

A_2 Crankshaft angular acceleration

A_{2I} Crankshaft angular acceleration at the start of a rotational increment

DBB Distance between the main and cage bearings.

DT Distance between the center of the throw bearing and the main bearing as measured parallel to the center line of the crankshaft

D_I Distance between the center of mass of the Ith unbalanced mass and the main bearing measured parallel to the center line of the crankshaft

e_U Eccentricity of unbalanced mass with respect to the center line of the crankshaft

F_{23X} Force exerted on the connecting rod in the X-direction by the crankshaft

F_{23Y} Force exerted on the connecting rod in the Y-direction by the crankshaft

F_{3PX} Force exerted on the piston in the X-direction by the connecting rod

F_{3PY} Force exerted on the piston in the Y-direction by the connecting rod

FCBX X-direction component of the force exerted on the crankshaft by the cage bearing

FCBY Y-direction component of the force exerted on the crankshaft by the cage bearing

FMBX X-direction component of the force exerted on the crankshaft by the main bearing

FMBY Y-direction component of the force exerted on the crankshaft by the bearing

FPRESS Force exerted on the sprung mass of the compressor due to pressure forces

F_R Radial component of the unbalanced force

FSIX Force exerted on the sprung mass of the compressor by spring I in the X-direction

FSIY Force exerted on the sprung mass of the compressor by spring I in the Y-direction

FSIZ Force exerted on the sprung mass of the compressor by spring I in the Z-direction

FSLX Force exerted on the sprung mass of the compressor by the shock loop in the X-direction

FSLY Force exerted on the sprung mass of the compressor by the shock loop in the Y-direction

FSLZ Force exerted on the sprung mass of the compressor by the shock loop in the Z-direction

F_T Tangential component of the unbalanced force

F_{WP} Force exerted on the piston normal to the wall

F_{YU} Y-direction component of the unbalanced force

I_{CR} Connecting rod moment of inertia about its center of gravity

I_{CSR} Moment of inertia of the crankshaft and rotor about their axis of rotation

I_X Moment of inertia of the sprung mass about an axis passing through its center of gravity parallel to the X-direction

I_Y Moment of inertia on the sprung mass about an axis passing through its center of gravity parallel to the Y-direction

I_Z Moment of inertia on the sprung mass about an axis passing through its center of gravity parallel to the Z-direction

KSIX Effective X-direction spring constant of spring I

KSIY Effective Y-direction spring constant of spring I

KSIZ Effective Z-direction spring constant of spring I

KSLX Effective X-direction spring constant of the shock loop

KSLY Effective Y-direction spring constant of the shock loop

KSLZ Effective Z-direction spring constant of the shock loop

L Length between connecting rod bearing centers

M Distance from crnakshaft bearing center of gravity

M_{CR} Connecting rod mass

M_P Piston mass

m Mass of sprung mass

m_U Unbalanced mass

$\Delta\theta$ Increment of crankshaft rotation

θ_X Rotational displacement of the sprung mass about the X-axis

θ_Y Rotational displacement of the sprung mass about the Y-axis

θ_Z Rotational displacement of the sprung mass about the Z-axis

Phase angle between the crankshaft throw and the radial location of the unbalanced mass

P Force exerted on the piston due to gas pressure

P_{CYL} Cylinder pressure

P_{SUC} Suction line pressure

R Crankshaft throw

R_C Cylinder radius

T Torque exerted on the rotor by the motor

W_2 Crankshaft angular velocity

W_{2I} Crankshaft angular velocity at the start of a rotational increment

X Linear displacement of the center of gravity of sprung mass in the X-direction

Y Linear displacement of the center of gravity of sprung mass in the Y-direction

Z Linear displacement of the center of gravity of sprung mass in the Z-direction

BIBLIOGRAPHY

1. Cowie, Alexander, "Kinematics and Design of Mechanisms," International Text Book Company, Scranton, PA, 1961

2. Meirovitch, Leonard, "Analytical Methods in Vibrations," MacMillan Company, New York, 1967

3. Gatecliff, G. W. and Lady, E.R., "Computation of Bearing and Unbalance Forces in Reciprocating Refrigeration Compressors," A.S.H.R.A.E. Paper No. 2206, presented at the Annual Meeting, Washington, D.C., August 22-25, 1971.